

OSDEnhancer: Taming Real-World Space-Time Video Super-Resolution with One-Step Diffusion

Shuoyan Wei^{1,2} Feng Li^{3,†} Chen Zhou^{1,2} Runmin Cong⁴ Yao Zhao^{1,2} Huihui Bai^{1,2}

¹Institute of Information Science, Beijing Jiaotong University ²Visual Intelligence +X International Cooperation Joint Laboratory of MOE

³School of Computer Science and Information Engineering, Hefei University of Technology ⁴School of Control Science and Engineering, Shandong University
 {shuoyan.wei, chenzhou, yzhao, hhbai}@bjtu.edu.cn, fengli@hfut.edu.cn, rmcong@sdu.edu.cn

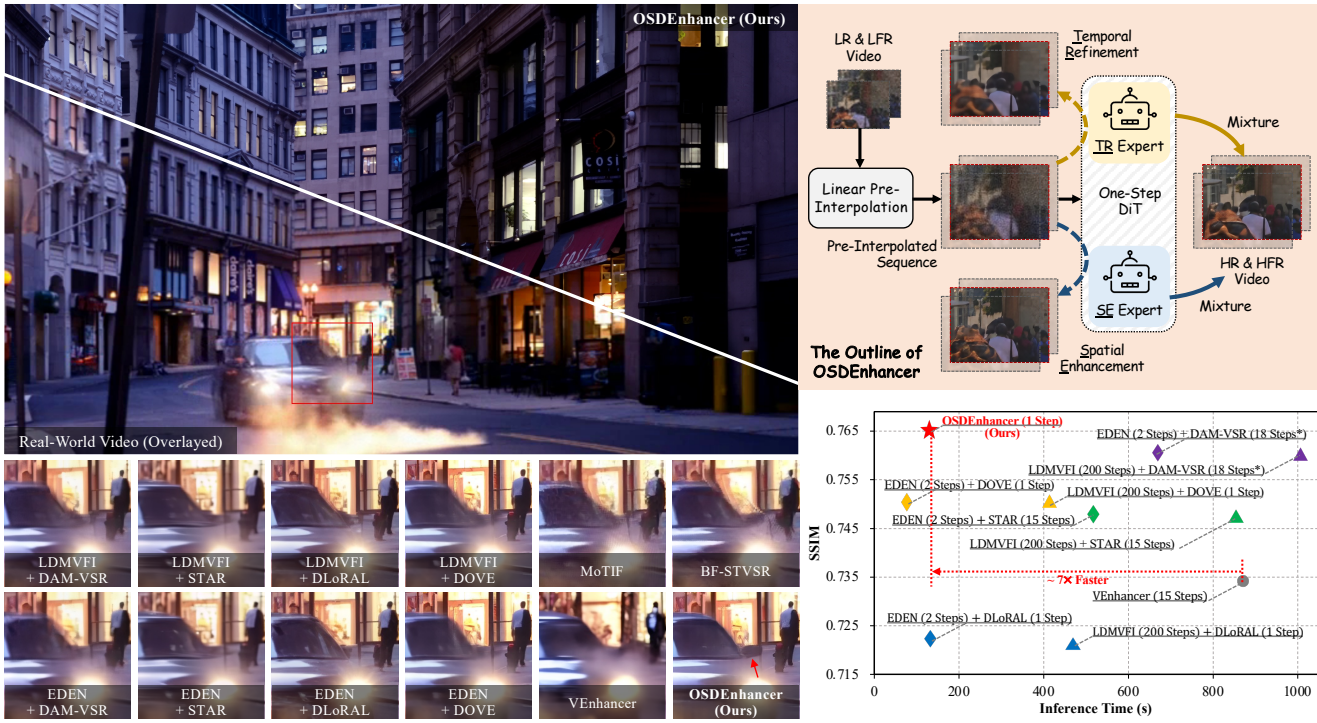


Figure 1. Performance and efficiency comparison on real-world STVSR. Our OSDEnhancer adopts a one-step diffusion framework with a temporal-refinement and spatial-enhancement mixture-of-experts (TR-SE MoE) architecture. OSDEnhancer demonstrates superior reconstruction on interpolated frames over the real-world VideoLQ dataset [3], exhibiting clearer structures and details. Moreover, it achieves higher fidelity and comparable efficiency than state-of-the-art DM-based methods on the real-world MVS4x dataset [46] under generating a 97-frame 1024×1024 video with single-frame interpolation, while delivering a $\sim 7\times$ speedup over the recent DM-based STVSR approach VEnhancer [16] on an NVIDIA A800 GPU. * DAM-VSR uses an extra DM of image super-resolution; only the main DM steps are reported.

Abstract

Diffusion models (DMs) have demonstrated exceptional success in video super-resolution (VSR), showcasing a powerful capacity for generating fine-grained details. However, their potential for space-time video super-resolution

(STVSR), which necessitates not only recovering realistic visual content from low-resolution to high-resolution but also improving the frame rate with coherent temporal dynamics, remains largely underexplored. Moreover, existing STVSR methods predominantly address spatiotemporal upsampling under simplified degradation assumptions, which often struggle in real-world scenarios with complex unknown degradations. Such a high demand for reconstruction fidelity and temporal consistency makes the develop-

[†]Corresponding author.

Demo video: <https://youtu.be/Qp93HvXNAi4>

ment of a robust STVSR framework particularly non-trivial. To address these challenges, we propose OSDEnhancer, a novel framework that, to the best of our knowledge, represents the first method to achieve real-world STVSR through an efficient one-step diffusion process. OSDEnhancer initializes essential spatiotemporal structures through a linear pre-interpolation strategy and pivots on training temporal refinement and spatial enhancement mixture of experts (TR-SE MoE), which allows distinct expert pathways to progressively learn robust, specialized representations for temporal coherence and spatial detail, further collaboratively reinforcing each other during inference. A bidirectional deformable variational autoencoder (VAE) decoder is further introduced to perform recurrent spatiotemporal aggregation and propagation, enhancing cross-frame reconstruction fidelity. Experiments demonstrate that the proposed method achieves state-of-the-art performance while maintaining superior generalization capability in real-world scenarios.

1. Introduction

Video rescaling across spatial and temporal resolution is widely employed in video streaming and continuous media data [28, 34, 42] to ensure cross-device compatibility, efficient transmission, and storage savings, often at the expense of reduced spatial resolution and temporal frame rates. This necessity has raised the development of video super-resolution (VSR) [38, 59, 66] and video frame interpolation (VFI) [1, 21, 36] techniques, which perform spatial or temporal upscaling in isolation, overlooking their intrinsic correlations.

Space-time video super-resolution (STVSR) [5, 55, 56, 58] handles the shortcomings by reconstructing a high-resolution (HR), high-frame-rate (HFR) video from its low-resolution (LR), low-frame-rate (LFR) counterpart within a unified model, thereby presenting visually appealing high-definition or even ultra-high-definition content. Nevertheless, existing methods [4, 24, 50, 67] are primarily designed for ideal and known degradations (*e.g.*, bicubic downsampling), lacking sufficient attention to heterogeneous unexpected degradations, such as noise, blurs, compression artifacts, and camera sensor imperfections that characterize real-world scenarios. Recent studies [14, 25, 33] have increasingly focused on real-world VSR by crafting complex degradation pipelines [3, 7, 46], especially empowered by diffusion models (DMs) [12, 35, 62] for their strong generative capability in realistic detail synthesis [11, 29, 30, 45, 61, 69]. Therefore, a straightforward solution might cascade independent VFI and real-world VSR models. However, as illustrated in Fig. 1, such execution still falls short in reconstructing structural fidelity.

Despite the above discussion, we have also found that

the majority of current DM-based VSR [11, 29, 45, 69] and VFI [22, 37, 60, 70] methods inherit the multi-step sampling trajectory from their pre-trained foundations, making inference slow and deployment impractical, particularly when confronted with long sequences or resource constraints. This indicates that the path to efficient STVSR is not as straightforward. Recent VSR methods [7, 30, 40] reformulate diffusion to enable one-step inference, leveraging the degraded video as a direct starting point. Yet, this approach faces a fundamental barrier in STVSR, where the simultaneous absence of target intermediate frames and HR details creates compounded additional ambiguity in space and time, rendering efficient and robust STVSR significantly non-trivial.

To address these challenges, we propose a novel DM-based framework, termed OSDEnhancer, which transcends prior limitations to achieve temporally consistent and high-fidelity generation for real-world STVSR in an efficient one-step sampling paradigm. OSDEnhancer begins with a linear pre-interpolation strategy that initializes coarse intermediate frames, establishing essential spatiotemporal structures. Building upon the powerful generative prior of pre-trained video diffusion models (VDMs) [17, 62], a divide-and-conquer strategy is orchestrated around it. Specifically, OSDEnhancer disentangles STVSR into complementary temporal refinement and spatial enhancement (TR-SE) equipped with the corresponding mixture-of-experts (MoE), where such specialized experts share the same pre-trained diffusion transformer (DiT) [62] but are progressively fine-tuned to tackle spatial and temporal degradations. To further reinforce inter-frame coherence, we not only utilize temporal residuals to focus the TR expert on regions of pronounced inter-frame variations but also incorporate residual-aware supervision to facilitate motion modeling. We finally integrate a bidirectional deformable variational autoencoder (VAE) decoder that enhances latent-to-pixel reconstruction by jointly performing multi-scale deformable aggregation and inter-frame feature propagation via deformable recurrent blocks. It performs recurrent propagation within each scale, with the temporal direction alternated across adjacent scales, enabling effective bidirectional compensation. In this way, our method eliminates the reliance on multi-network distillation [30, 40] or adversarial training [44] required by previous one-step approaches, ensuring both temporal consistency and generative realism in more stable and efficient one-step inference while maintaining strong robustness to real scenarios. The main contributions are as follows:

- We propose OSDEnhancer, to the best of our knowledge, as the first DM-based STVSR approach achieving one-step inference. Extensive experiments validate the superiority of OSDEnhancer across various degradations, demonstrating temporally consistent and high-fidelity re-

construction.

- We propose the TR-SE MoE, which disentangles and addresses temporal and spatial degradations while progressively optimizing specialized representations for both in a divide-and-conquer manner.
- We design a bidirectional deformable VAE decoder that performs multi-scale deformable aggregation and inter-frame feature propagation to strengthen the latent-to-pixel reconstruction and inter-frame consistency in STVSR.

2. Related Work

2.1. Space-Time Video Super-Resolution (STVSR)

STVSR methods usually apply optical flow [15, 20], deformable kernels [55, 58], or transformers [13, 19] to synthesize latent spatiotemporal features. To acquire continuous inter-frame features, VideoINR [5] combines implicit neural representations with optical flow. MoTIF [4] encodes sparsely sampled forward motion as contextual input to ease motion interpolation. BF-STVSR [24] introduces a B-spline mapper for smooth temporal interpolation. However, these approaches typically adopt simplified degradation assumptions (*e.g.*, bicubic downsampling), which limit their applicability to complex degradations. In addition, their reliance on discriminative models constrains the synthesis of realistic texture details. Instead, VEnhancer [16] pioneers DM-based STVSR by conditioning a pretrained text-to-video model on low-quality videos via ControlNet [64]. Although capable of generating rich visual details, the heavy use of textual conditioning introduces notable stochasticity, which compromises reconstruction fidelity. Besides, its reliance on multi-step diffusion results in high inference latency. The research on one-step diffusion for STVSR remains unexplored.

2.2. Real-World Video Super-Resolution (VSR)

To tackle real-world degradations, image diffusion models (IDMs) and video diffusion models (VDMs) have recently shown strong performance in VSR [14, 61, 69] by leveraging powerful generative priors. These approaches generally require constraints to preserve reconstruction fidelity: IDMs [29, 30, 61] incorporate temporal layers to enforce consistency across frames, while VDMs [6, 25, 57] typically leverage ControlNet [64] to condition and constrain video generation. To improve efficiency, later works accelerate multi-step diffusion to one-step inference via adversarial training [44], score distillation [30, 40], or flow matching [72], often at the cost of training stability and fidelity. In contrast, DOVE [7] achieves better fidelity in real-world VSR by adopting a latent-pixel training strategy with purely regression objectives. Nevertheless, compared with VSR, STVSR lacks critical latent inter-frame information, making it challenging for one-step diffusion models to jointly

model spatial and temporal degradations.

2.3. Video Frame Interpolation (VFI)

VFI focuses on synthesizing intermediate frames between given inputs and is closely related to temporal modeling in STVSR. Recent DM-based VFI methods [22, 37, 60, 70] capture motion and occlusion uncertainty through generative sampling, leading to improved visual quality and generalization. For instance, LDMVFI [9] formulates VFI as a conditional generation problem within a latent diffusion framework, significantly enhancing perceptual quality. MoMo [27] further improves visual fidelity by explicitly modeling intermediate motion. More recently, EDEN [68] adopts a diffusion transformer with temporal attention and a start-end frame difference embedding, achieving state-of-the-art performance on large-motion video benchmarks. However, the inherent absence of explicit inter-frame structural representations poses a fundamental challenge for one-step diffusion in VFI, and the direct integration of VFI and VSR for STVSR often leads to redundant and inefficient formulations.

3. Method

We present OSDEnhancer, a one-step diffusion framework for real-world STVSR. Sec.3.1 first reviews the relevant preliminaries. Then, we introduce the overall architecture of OSDEnhancer in Sec.3.2, followed by the temporal-refinement and spatial-enhancement mixture-of-experts (TR-SE MoE) in Sec.3.3. Sec.3.4 finally presents the bidirectional deformable VAE decoder.

3.1. Preliminary

We adopt the powerful pretrained CogVideoX [62] as the backbone in OSDEnhancer. CogVideoX utilizes a 3D causal variational autoencoder (VAE) to compress a video into latent code \mathbf{z} and employs a transformer to perform the diffusion process. In the forward process, a clean latent code \mathbf{z}_0 is progressively noised into \mathbf{z}_t by Gaussian noise ϵ : $\mathbf{z}_t = \sqrt{\bar{\alpha}_t} \mathbf{z}_0 + \sqrt{1 - \bar{\alpha}_t} \epsilon$, where $\bar{\alpha}_t$ is the predefined schedule factor at timestep t . Given that the input video already provides structural information rather than pure noise, following prior VSR methods [7, 53, 54], we treat the encoded input video sequence \mathbf{z}^{in} as the starting point of the diffusion process and produce the target video sequence \mathbf{z}^{out} . Under the v -prediction formulation of CogVideoX, the denoising process can be expressed as

$$\mathbf{z}^{\text{out}} = \sqrt{\bar{\alpha}_t} \mathbf{z}^{\text{in}} - \sqrt{1 - \bar{\alpha}_t} \mathbf{v}_\theta(\mathbf{z}^{\text{in}}, \mathbf{c}, t), \quad (1)$$

where \mathbf{v}_θ denotes the predicted velocity under condition \mathbf{c} and t using a diffusion transformer (DiT).

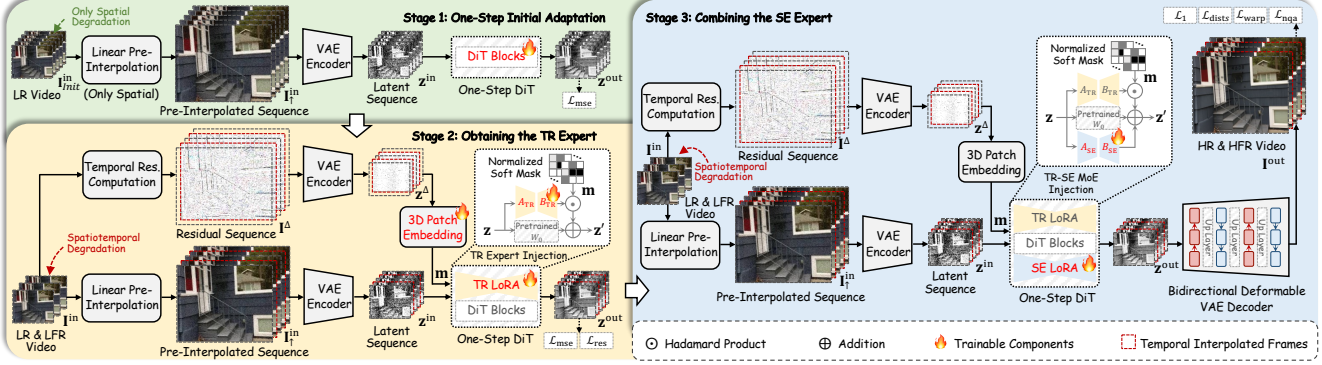


Figure 2. The overall training pipeline of the proposed OSDEnhancer framework. Our method aims to generate an HR and HFR video with high fidelity and rich detail from a LR and LFR one via one-step diffusion. Specifically, we adopt the TR-SE MoE with progressive training to explicitly disentangle temporal and spatial degradations.

3.2. Overall framework

The overall framework of OSDEnhancer is illustrated in Fig. 2. Our key insight lies in transcending the limitations of current STVSR methods, enabling a one-step diffusion framework for real-world scenarios. Given a LR and LFR video sequence $\mathbf{I}^{\text{in}} = \{I_{2n-1}^{\text{in}}\}_{n=1}^N$, our goal is to generate a HR and HFR version $\mathbf{I}^{\text{out}} = \{I_1^{\text{out}}, I_2^{\text{out}}, \dots, I_{2(1)}^{\text{out}}, I_3^{\text{out}}, \dots, I_{2N-1}^{\text{out}}\}$, where K denotes the number of temporally interpolated frames between two consecutive input frames. For example, $\{I_{2n(k)}^{\text{in}}\}_{k=1}^K$ indicates the interpolated frame between I_{2n-1}^{in} and I_{2n+1}^{in} .

Unlike VSR, directly adapting a pre-trained VDM to the STVSR task presents a distinct challenge. The input in STVSR is fundamentally undersampled, suffering from compounded spatiotemporal ambiguity as it is simultaneously devoid of target high-resolution details and the requisite intermediate frames. According to Eq. (1), the denoising process from \mathbf{z}^{in} to \mathbf{z}^{out} tends to preserve the dimensionality of the latent space. Therefore, the issues of spatial resolution alignment and inter-frame completion must be addressed before denoising. To this end, we apply a linear pre-interpolation strategy on \mathbf{I}^{in} before VAE encoding, generating a spatiotemporal-aligned sequence $\mathbf{I}_{\uparrow}^{\text{in}}$. Specifically, for the potential intermediate frame $\{I_{2n(k)}^{\text{in}}\}_{k=1}^K$, we perform a weighted blending based on its relative temporal distances to I_{2n-1}^{in} and I_{2n+1}^{in} , formulated as

$$I_{2n(k)}^{\text{in}} = \frac{K+1-k}{K+1} I_{2n-1}^{\text{in}} + \frac{k}{K+1} I_{2n+1}^{\text{in}}. \quad (2)$$

This can efficiently replenish the inter-frame clues in the given LFR sequence with minimal computational overhead. Then, we perform spatial bilinear upsampling to obtain $\mathbf{I}_{\uparrow}^{\text{in}}$. We further compute the residuals between adjacent spatially unsampled input frames I_{2n-1}^{in} and I_{2n+1}^{in} to acquire a residual sequence \mathbf{I}^{Δ} whose temporal length is aligned with $\mathbf{I}_{\uparrow}^{\text{in}}$,

defined as

$$I_{2n(k)}^{\Delta} = \text{Up}(I_{2n+1}^{\text{in}}) - \text{Up}(I_{2n-1}^{\text{in}}), \quad (3)$$

where $\text{Up}(\cdot)$ denotes the upsampling operation and $I_{2n-1}^{\Delta} = 0$.

Then, $\mathbf{I}_{\uparrow}^{\text{in}}$ and \mathbf{I}^{Δ} are fed into the VAE encoder to produce the latent sequence \mathbf{z}^{in} and \mathbf{z}^{Δ} , respectively. OSDEnhancer employs the temporal refinement and spatial enhancement mixture-of-experts (TR-SE MoE), which progressively fine-tunes the pre-trained DiT to enhance both temporal consistency and spatial detail. Notably, the temporal residuals serve not only as input to the TR expert to supply inter-frame information but also as a consistency supervision signal to facilitate motion modeling. Subsequently, A one-step DiT predicts the velocity \mathbf{v}_{θ} to obtain the latent sequence \mathbf{z}^{out} , where \mathbf{z}^{Δ} is considered part of the condition \mathbf{c} . Finally, \mathbf{z}^{out} is decoded by our bidirectional deformable VAE decoder to generate the final output \mathbf{I}^{out} .

3.3. TR-SE MoE

The overwhelming burden in DM-based STVSR stems from its coupled constraints: a unified framework must jointly address temporal interpolation and spatial restoration, which becomes particularly stringent under a one-step sampling paradigm. To overcome this challenge, OSDEnhancer adopts a divide-and-conquer approach, decoupling the task into temporal refinement and spatial enhancement (TR-SE). This is implemented via a corresponding mixture-of-experts (MoE) model. Concretely, the distinct experts are built upon the same pre-trained DiT to specialize in handling temporal and spatial degradations through progressive multi-stage fine-tuning.

Stage 1: Initial One-Step Adaptation. The original pre-trained DiT is designed for multi-step inference. To facilitate its adaptation to our one-step setting, we initially fine-tune DiT on paired data $\{\mathbf{I}_{\text{Init}}^{\text{in}}, \mathbf{I}^{\text{gt}}\}$ with only spatial degra-

ditions. As the latent space compactly encodes spatiotemporal information, we employ the MSE loss \mathcal{L}_{mse} as the regression objective in the latent domain:

$$\mathcal{L}_{\text{Stage1}} = \mathcal{L}_{\text{mse}}(\mathbf{z}^{\text{out}}, \mathbf{z}^{\text{gt}}), \quad (4)$$

where \mathbf{z}^{gt} is the latent code of the ground-truth (GT) sequence \mathbf{I}^{gt} .

Stage 2: Obtaining the TR Expert. Based on the one-step adapted DiT from Stage 1, we construct a temporal-refinement (TR) expert by augmenting DiT with LoRA [18]. To specialize it for temporal degradations, the input video sequence \mathbf{I}^{in} is derived by applying temporal subsampling to $\mathbf{I}_{\text{Init}}^{\text{in}}$. The TR expert learns low-rank decomposition matrices A_{TR} and B_{TR} , whose output is modulated via a Hadamard product with a normalized soft mask \mathbf{m} calculated from the residual latent sequence \mathbf{z}^{Δ} , before being injected back into the backbone. This design enables the TR expert to selectively enhance regions with pronounced inter-frame variation, thereby facilitating temporal consistency. This process is formulated as

$$\mathbf{z}' = W_0 \mathbf{z} + \mathbf{m} \odot B_{\text{TR}} A_{\text{TR}} \mathbf{z}, \quad (5)$$

where \odot denotes the Hadamard product; \mathbf{z}' and W_0 represent the original weight and the output of the network component, respectively. The normalized soft mask \mathbf{m} is calculated from \mathbf{z}^{Δ} by 3D patch embedding. At this stage, the network parameters are frozen except for A_{TR} , B_{TR} , and the 3D residual patch embedding modules. In this stage, besides the MSE loss, we also introduce a residual-aware supervision \mathcal{L}_{res} that constrains the distance between consecutive residuals in the predicted latent sequence \mathbf{z}^{out} and those in the ideal latent sequence \mathbf{z}^{gt} , described as

$$\mathcal{L}_{\text{Stage2}} = \mathcal{L}_{\text{mse}}(\mathbf{z}^{\text{out}}, \mathbf{z}^{\text{gt}}) + \lambda_{\text{res}} \mathcal{L}_{\text{res}}(\mathbf{z}^{\text{out}}, \mathbf{z}^{\text{gt}}), \quad (6)$$

where λ_{res} is a hyper-parameter that balances the residual loss.

Stage 3: Combining the SE Expert. Learning in the latent space enables efficient and faithful representation learning. However, the inherent compression limits the recovery of fine-grained details in pixel-space outputs. Fully fine-tuning the DiT for this purpose is computationally prohibitive. Therefore, we introduce a spatial-enhancement (SE) expert, instantiated by additional low-rank decomposition matrices A_{SE} and B_{SE} to operate and refine the spatial details. Combined with the previous TR expert, the injected network component yields a mixed output as

$$\mathbf{z}' = W_0 \mathbf{z} + \mathbf{m} \odot B_{\text{TR}} A_{\text{TR}} \mathbf{z} + B_{\text{SE}} A_{\text{SE}} \mathbf{z}. \quad (7)$$

In this manner, the TR and SE experts complement each other to achieve effective STVSR. The optimization at this stage incorporates losses from several aspects. For reconstruction fidelity and structural similarity, we employ the L1

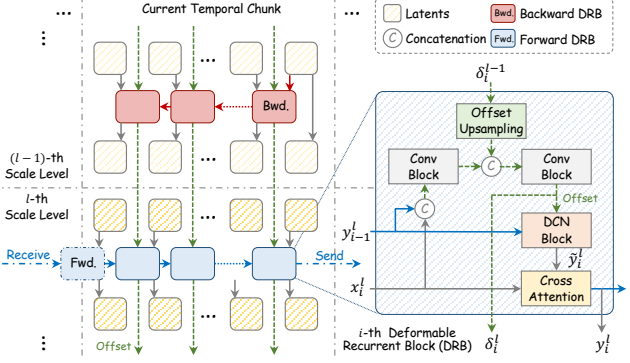


Figure 3. The illustration of the bidirectional deformable VAE decoder pipeline. Deformable recurrent blocks (DRBs) integrated into the upsampling layers of a 3D causal VAE decoder [62], enabling multi-scale cross-frame compensation.

loss \mathcal{L}_1 and the DISTS loss $\mathcal{L}_{\text{dists}}$ [10]. To enforce temporal consistency, a self-supervised optical-flow warping loss $\mathcal{L}_{\text{warp}}$ [26] is applied to the high-frequency components of the output. In addition, to enhance perceptual quality, we adopt a no-reference quality assessment loss \mathcal{L}_{nqa} [23] as a regularization term to optimize the experts. The overall loss function for this stage is formulated as

$$\mathcal{L}_{\text{Stage3}} = \mathcal{L}_1(\mathbf{I}^{\text{out}}, \mathbf{I}^{\text{gt}}) + \lambda_{\text{dists}} \mathcal{L}_{\text{dists}}(\mathbf{I}^{\text{out}}, \mathbf{I}^{\text{gt}}) + \lambda_{\text{warp}} \mathcal{L}_{\text{warp}}(\mathbf{I}^{\text{out}}) - \lambda_{\text{nqa}} \mathcal{L}_{\text{nqa}}(\mathbf{I}^{\text{out}}), \quad (8)$$

where λ_{dists} , λ_{warp} , and λ_{nqa} are loss weights.

3.4. Bidirectional Deformable VAE Decoder

While 3D VAEs in VDMs typically employ temporally causal convolutions to capture inter-frame dependencies, this inherently restricts information flow to past frames. However, STVSR involves the temporal interpolation between consecutive frames, where output frames temporally aligned with the inputs often yield more accurate and faithful reconstructions. The strict temporal causality further limits effective global compensation from these frames during decoding. To address this issue, we propose a bidirectional deformable VAE decoder. As shown in Fig. 3, the decoder integrates deformable recurrent blocks (DRBs) into the upsampling layers of the original 3D causal VAE decoder to learn multi-scale deformable aggregation and inter-frame feature propagation.

Specifically, at each l -th scale level, for the i -th DRB, the output y_{i-1}^l from the previous $(i-1)$ -th DRB is first paired with the current input x_i^l to estimate the deformation offset through a convolutional block. Inspired by the PCD network [47], we further propagate the upsampled offset δ_i^{l-1} at the lower scale level $(l-1)$ to the current level to obtain a more reliable and expressive offset δ_i^l . Then, δ_i^l is used in a deformable convolution block $\text{DCN}(\cdot)$ [71] applied to y_{i-1}^l ,

producing the aligned feature \tilde{y}_{i-1}^l with respect to x_i^l . Finally, a cross-attention $\text{attn}(\cdot)$ is employed to compensate the current x_i^l with information propagated from the neighboring aligned feature \tilde{y}_{i-1}^l to get y_i^l . This process can be formulated as

$$\begin{aligned}\delta_i^l &= \text{conv}(\text{conv}(x_i^l, y_{i-1}^l), \text{Up}(\delta_{i-1}^{l-1})), \\ \tilde{y}_{i-1}^l &= \text{DCN}(y_{i-1}^l, \delta_i^l), \quad y_i^l = \text{attn}(x_i^l, \tilde{y}_{i-1}^l),\end{aligned}\quad (9)$$

where $\text{conv}(\cdot, \cdot)$ denotes the operation of applying a convolutional block after channel-wise concatenation. To reduce the computational overhead of bidirectional compensation, recurrent propagation within each scale level is performed in a single temporal direction, while the propagation direction is reversed at the next scale level. Hence, we can preserve the original temporal chunking scheme for long video processing. Forward information is propagated globally, whereas backward information is restricted to temporal chunks, achieving efficient bidirectional compensation with reduced latency and controlled error accumulation.

During training, we optimize only the DRBs on the high-quality (HQ) video dataset (*i.e.*, HQ-VSR [7]) using the reconstruction loss and perception loss adopted in the original VAE [62], while additionally enforcing inter-frame consistency in the pixel space via the residual loss \mathcal{L}_{res} .

4. Experiments

4.1. Experimental Settings

Datasets. To support our multi-stage training scheme, we employ HQ-VSR [7], Adobe240 [39], and DIV2K [2] as HQ video, HFR video, and HQ image datasets, respectively. Spatial degradations are synthesized using the RealBasicVSR [3] pipeline, while the original data serve as the GT. In Stage 1, we use the HQ-VSR dataset with only spatial degradation. In Stage 2, the Adobe240 dataset is subjected to both spatial and temporal degradations, where temporal degradation is conducted by uniformly skipping 0, 1, 3, 7, or 15 frames. In Stage 3, we adopt a mixture of HQ-VSR videos and DIV2K images (with images duplicated to match video length) and apply spatial degradation together with mild temporal degradation by uniformly skipping 0 or 1 frame. For evaluation, we comprehensively consider both synthetic and real-world datasets. The synthetic benchmarks include UDM10 [41], SPMCS [63], YouHQ40 [69], and GoPro [32], while the real-world datasets comprise MVSR4x [46] and VideoLQ [3], where synthetic degradation processes are consistent with the training settings. Following previous STVSR work [24], we evaluate STVSR performance at multiple spatiotemporal scales on the HFR GoPro dataset. For other datasets with lower frame rates, we only consider single-frame interpolation with $4\times$ spatial upscaling, unless otherwise specified.

Implementation Details. We adopt the text-to-video model, CogVideoX1.5-5B [62], as the pretrained backbone to implement our OSDEnhancer. To stabilize generation and reduce redundant text encoding overhead, we follow [7] and consistently use empty text embeddings as conditions. Training is conducted on 4 NVIDIA RTX PRO 6000 GPUs with a batch size of 4. *More details can be found in the supplementary.*

Evaluation Metrics. We employ a diverse set of quality metrics to comprehensively evaluate STVSR performance. Specifically, we report full-reference metrics PSNR and SSIM [49], as well as perceptual metrics LPIPS [65]. To further assess perceptual similarity with respect to inter-frame motion consistency, we adopt FloLPIPS [8]. Moreover, we employ no-reference image quality assessment (IQA) metrics, including MUSIQ [23] and CLIP-IQA [43], together with no-reference video quality assessment (VQA) metrics, namely FasterVQA [51] and DOVER [52]. For datasets without GT, such as VideoLQ [3], we only report IQA and VQA metrics.

4.2. Comparison with State-of-the-Art Methods

We compare our OSDEnhancer with state-of-the-art STVSR methods: 1) two-stage STVSR methods that integrate video frame interpolation (VFI) methods, including LDMVFI [9] and EDEN [68], with video super-resolution (VSR) methods, including DAM-VSR [25], STAR [57], DLoRAL [40], and DOVE [7]; and 2) one-stage STVSR methods, including VideoINR [5], MoTIF [4], BF-STVSR [24], and VEnhancer [16]. Notably, since VideoINR, MoTIF, and BF-STVSR are non-DM-based methods developed under the bicubic downsampling assumption, we retrain these methods using the same degradation setting as ours to ensure a fair comparison.

Quantitative Comparison. The quantitative results on multiple datasets are reported in Tab. 1. Benefiting from the joint design of temporal refinement and spatial enhancement, OSDEnhancer achieves consistently superior performance across almost all datasets in most metrics. It attains the overall best scores on both IQA and VQA measures under synthetic and real-world degradations, demonstrating robust generalization. While DLoRAL [40] achieves higher CLIP-IQA scores, indicating better semantic alignment, it lags significantly behind our method in terms of reconstruction fidelity (*e.g.*, PSNR and SSIM). Moreover, DM-based VFI methods like LDMVFI [9] and EDEN [68], which lack native multi-frame interpolation support and suffer from error accumulation in recursive settings, perform notably worse than our method on GoPro [32] under multi-frame settings.

To further evaluate generalization across different spatial and temporal scales, we compare recent state-of-the-art continuous STVSR methods on the GoPro dataset [32], as

Table 1. Quantitative comparisons on multiple datasets, including synthetic datasets UDM10 [41], SPMCS [63], YouHQ40 [69], and GoPro [32], and real-world datasets MVS4x [46] and VideoLQ [3]. The spatial upscaling scale is $4\times$. GoPro adopts 7-frame interpolation; the other datasets adopt single-frame interpolation. Red, blue, and dark blue indicate the best, second-best, and third-best performances, respectively.

Datasets	Metrics	LDMVFI [9]			EDEN [68]			VideoINR [5]	MoTIF [4]	BF-STVSR [24]	VEnhancer [16]	OSDEnhancer (Ours)		
		DAM-VSR [25]	STAR [57]	DLoRAL [40]	DOVE [7]	DAM-VSR [25]	STAR [57]	DLoRAL [40]	DOVE [7]					
UDM10	PSNR \uparrow	25.19	24.04	22.38	26.37	25.12	23.97	22.32	26.36	25.10	24.97	25.09	21.64	26.44
	SSIM \uparrow	0.736	0.686	0.670	0.766	0.736	0.686	0.665	0.765	0.714	0.703	0.715	0.679	0.775
	LPIPS \downarrow	0.438	0.429	0.350	0.279	0.441	0.426	0.354	0.279	0.360	0.376	0.356	0.451	0.248
	FloLPIPS \downarrow	0.428	0.426	0.349	0.282	0.435	0.426	0.353	0.284	0.359	0.380	0.357	0.428	0.253
	MUSIQ \uparrow	31.77	36.60	63.55	60.70	31.38	36.26	63.83	60.87	41.18	42.67	43.51	33.55	65.95
	CLIP-IQA \uparrow	0.196	0.248	0.636	0.463	0.196	0.247	0.636	0.462	0.266	0.287	0.282	0.272	0.490
	FasterVQA \uparrow	0.364	0.591	0.758	0.764	0.388	0.597	0.763	0.760	0.583	0.668	0.678	0.524	0.805
SPMCS	DOVER \uparrow	0.368	0.441	0.723	0.770	0.369	0.466	0.723	0.776	0.447	0.547	0.525	0.447	0.796
	PSNR \uparrow	22.32	21.31	21.43	22.98	22.24	21.30	21.39	22.97	22.83	22.68	22.85	19.40	23.27
	SSIM \uparrow	0.579	0.537	0.541	0.614	0.577	0.538	0.540	0.614	0.593	0.588	0.594	0.502	0.617
	LPIPS \downarrow	0.582	0.555	0.346	0.293	0.592	0.550	0.346	0.294	0.406	0.390	0.394	0.533	0.288
	FloLPIPS \downarrow	0.530	0.514	0.323	0.273	0.543	0.515	0.331	0.275	0.381	0.362	0.368	0.510	0.270
	MUSIQ \uparrow	29.16	34.79	66.22	69.18	28.57	35.56	66.46	69.15	43.75	48.38	46.24	41.67	72.61
	CLIP-IQA \uparrow	0.209	0.265	0.572	0.519	0.207	0.262	0.571	0.519	0.241	0.289	0.273	0.326	0.535
YouHQ40	FasterVQA \uparrow	0.277	0.391	0.749	0.720	0.279	0.423	0.738	0.720	0.531	0.649	0.599	0.454	0.777
	DOVER \uparrow	0.226	0.301	0.672	0.778	0.222	0.308	0.669	0.781	0.422	0.512	0.495	0.399	0.792
	PSNR \uparrow	23.98	22.74	21.46	24.22	23.96	22.74	21.43	24.21	23.66	23.50	23.54	20.63	24.24
	SSIM \uparrow	0.665	0.641	0.585	0.675	0.665	0.640	0.583	0.675	0.639	0.628	0.635	0.600	0.678
	LPIPS \downarrow	0.442	0.467	0.357	0.300	0.442	0.469	0.357	0.300	0.404	0.392	0.391	0.487	0.287
	FloLPIPS \downarrow	0.428	0.445	0.357	0.304	0.428	0.446	0.358	0.304	0.396	0.388	0.388	0.463	0.289
	MUSIQ \uparrow	37.03	33.63	66.28	60.82	37.16	33.64	66.46	60.88	37.83	46.30	43.86	40.06	65.66
GoPro	CLIP-IQA \uparrow	0.248	0.275	0.613	0.446	0.248	0.275	0.613	0.447	0.274	0.332	0.306	0.333	0.495
	FasterVQA \uparrow	0.709	0.568	0.840	0.857	0.708	0.565	0.848	0.856	0.696	0.788	0.777	0.688	0.886
	DOVER \uparrow	0.615	0.580	0.822	0.851	0.616	0.580	0.824	0.850	0.652	0.728	0.739	0.675	0.867
	PSNR \uparrow	24.07	22.69	22.13	23.29	23.93	22.63	22.09	23.26	24.06	23.96	24.28	19.74	24.53
	SSIM \uparrow	0.706	0.652	0.611	0.668	0.701	0.648	0.612	0.667	0.687	0.675	0.696	0.575	0.716
	LPIPS \downarrow	0.412	0.463	0.328	0.294	0.423	0.462	0.328	0.298	0.272	0.277	0.271	0.541	0.269
	FloLPIPS \downarrow	0.408	0.456	0.328	0.291	0.418	0.453	0.328	0.294	0.268	0.277	0.265	0.535	0.263
MVS4x	MUSIQ \uparrow	35.42	30.87	62.49	62.09	35.04	32.90	62.61	61.53	37.02	41.18	43.25	27.74	66.75
	CLIP-IQA \uparrow	0.203	0.237	0.454	0.420	0.202	0.233	0.448	0.414	0.194	0.220	0.217	0.244	0.415
	FasterVQA \uparrow	0.538	0.480	0.801	0.811	0.514	0.458	0.791	0.798	0.540	0.660	0.709	0.477	0.838
	DOVER \uparrow	0.359	0.322	0.619	0.674	0.360	0.326	0.632	0.669	0.386	0.467	0.506	0.343	0.651
	PSNR \uparrow	23.19	22.52	21.88	22.30	23.20	22.51	21.89	22.28	21.40	20.88	21.61	20.87	22.71
	SSIM \uparrow	0.760	0.748	0.721	0.751	0.761	0.748	0.722	0.750	0.708	0.730	0.749	0.734	0.765
	LPIPS \downarrow	0.458	0.410	0.377	0.348	0.459	0.411	0.376	0.349	0.460	0.476	0.460	0.440	0.342
VideoLQ	FloLPIPS \downarrow	0.435	0.409	0.366	0.345	0.434	0.411	0.361	0.346	0.443	0.473	0.468	0.399	0.344
	MUSIQ \uparrow	24.35	29.70	62.56	62.69	24.11	30.06	62.27	62.58	37.71	33.41	22.09	35.22	62.65
	CLIP-IQA \uparrow	0.217	0.257	0.661	0.521	0.221	0.256	0.656	0.524	0.429	0.322	0.283	0.318	0.514
	FasterVQA \uparrow	0.211	0.264	0.738	0.775	0.199	0.279	0.741	0.775	0.583	0.575	0.294	0.332	0.778
VideoLQ	DOVER \uparrow	0.160	0.204	0.639	0.706	0.156	0.202	0.632	0.702	0.293	0.244	0.150	0.276	0.665
	MUSIQ \uparrow	34.61	39.14	60.00	43.84	34.02	39.17	59.76	43.93	30.94	35.79	34.89	39.38	45.30
	CLIP-IQA \uparrow	0.210	0.289	0.574	0.287	0.208	0.290	0.572	0.286	0.213	0.250	0.222	0.303	0.351
	FasterVQA \uparrow	0.625	0.663	0.753	0.718	0.624	0.673	0.755	0.721	0.579	0.661	0.646	0.639	0.765
	DOVER \uparrow	0.631	0.712	0.747	0.748	0.619	0.712	0.748	0.751	0.622	0.688	0.666	0.665	0.749

Table 2. Quantitative comparison (PSNR \uparrow / LPIPS \downarrow / FloLPIPS \downarrow / MUSIQ \uparrow) with state-of-the-art continuous STVSR methods under different temporal and spatial scales on the GoPro dataset [32]. Red indicates the best performance.

Temporal Scale	Spatial Scale	VideoINR [5]	MoTIF [4]	BF-STVSR [24]	VEnhancer [16]	OSDEnhancer (Ours)
1× (0 interp.)	8×	23.37 / 0.408 / 0.401 / 21.96	23.43 / 0.377 / 0.374 / 22.57	23.57 / 0.361 / 0.357 / 22.56	21.56 / 0.545 / 0.532 / 19.91	24.05 / 0.302 / 0.295 / 65.77
	12×	22.23 / 0.546 / 0.537 / 16.39	22.32 / 0.466 / 0.460 / 18.36	22.34 / 0.466 / 0.460 / 16.73	20.12 / 0.622 / 0.613 / 18.64	22.97 / 0.353 / 0.341 / 67.45
	16×	21.14 / 0.622 / 0.614 / 14.15	21.14 / 0.530 / 0.526 / 15.64	21.14 / 0.534 / 0.531 / 13.95	19.78 / 0.690 / 0.675 / 14.38	21.95 / 0.412 / 0.396 / 65.13
6× (5 interp.)	8×	23.20 / 0.407 / 0.403 / 21.93	23.42 / 0.375 / 0.373 / 23.04	23.51 / 0.379 / 0.377 / 21.04	14.09 / 0.716 / 0.717 / 19.16	23.55 / 0.321 / 0.314 / 66.52
	12×	22.11 / 0.532 / 0.523 / 16.44	22.41 / 0.467 / 0.457 / 18.18	22.43 / 0.494 / 0.485 / 15.30	14.20 / 0.748 / 0.749 / 19.09	22.63 / 0.375 / 0.363 / 67.42
	16×	21.08 / 0.611 / 0.602 / 13.98	21.27 / 0.537 / 0.528 / 15.22	21.28 / 0.558 / 0.547 / 13.59	14.53 / 0.773 / 0.773 / 14.92	21.75 / 0.432 / 0.417 / 64.21
12× (11 interp.)	8×	22.47 / 0.413 / 0.411 / 21.65	22.63 / 0.388 / 0.393 / 22.65	22.81 / 0.403 / 0.405 / 20.15	13.68 / 0.737 / 0.738 / 19.01	22.25 / 0.350 / 0.347 / 66.74
	12×	21.54 / 0.527 / 0.520 / 16.51	21.86 / 0.477 / 0.473 / 17.96	21.94 / 0.515 / 0.512 / 15.10	13.72 / 0.759 / 0.760 / 19.17	21.62 / 0.399 / 0.392 / 66.40
	16×	21.54 / 0.606 / 0.600 / 13.99	20.97 / 0.545 / 0.540 / 15.06	21.02 / 0.574 / 0.568 / 13.80	14.07 / 0.784 / 0.784 / 15.33	21.05 / 0.450 / 0.440 / 63.30

shown in Tab. 2. It can be observed that OSDEnhancer maintains high fidelity while achieving superior temporal consistency and perceptual quality under large temporal gaps and high spatial scales, as evidenced by the best LPIPS, FloLPIPS, and an approximately 40 improvement

in MUSIQ.

Qualitative Comparison. Visual comparisons of single-frame and multi-frame interpolation with $4\times$ spatial upscaling are shown in Fig. 4 and Fig. 5. Consistent with the quantitative results, OSDEnhancer reconstructs sharper



Figure 4. Qualitative comparison of interpolated frames on real-world videos from VideoLQ [3]. Left: overlay of adjacent LR frames.

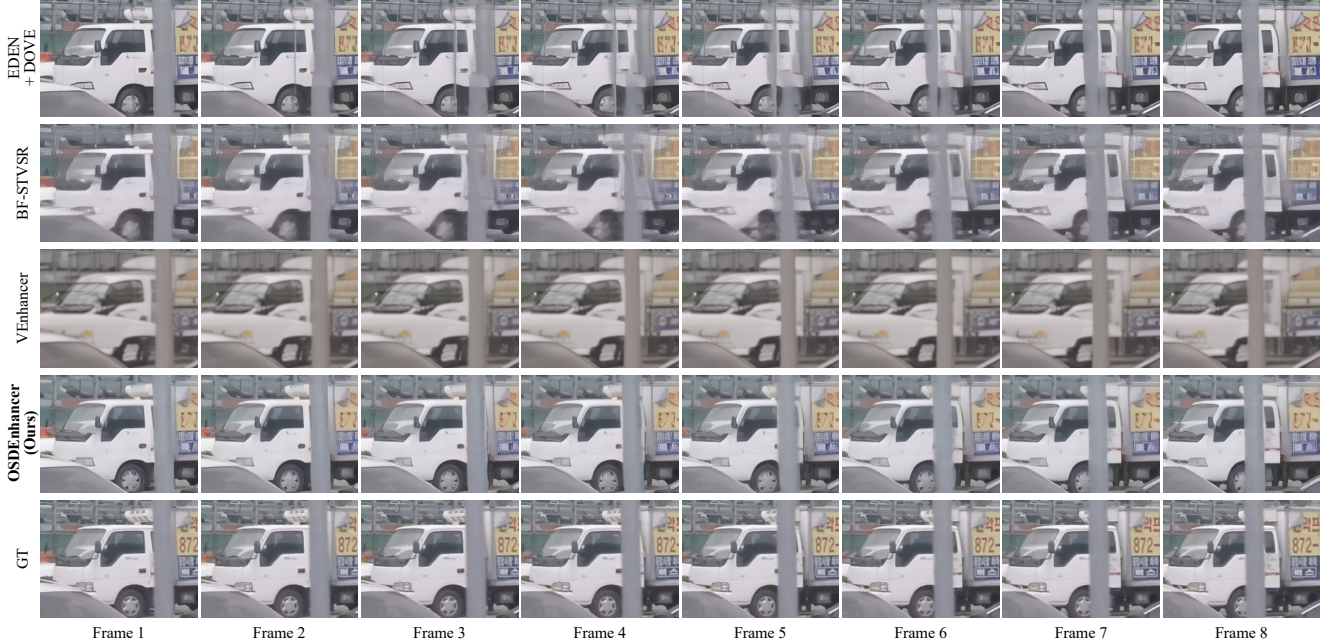


Figure 5. Qualitative comparison of STVSR on the GoPro dataset [32] with 4 \times spatial upscaling and 7-frame interpolation (frames 2–8 are interpolated).

structures and more faithful details while maintaining superior temporal consistency, whereas competing methods often exhibit over-smoothing, flickering, or motion-related artifacts. In particular, under large motion scales and non-linear dynamics, competing methods tend to lose fine details or produce blurred and distorted structures, while OSDEnhancer preserves sharper edges and more faithful spatial textures across frames.

Temporal Consistency Comparison. Beyond the quantitative FloLPIPS results reported in Tab. 1 and Tab. 2, we further evaluate temporal consistency using frame-wise temporal profiles in Fig. 6. Existing methods often suffer from flickering, misalignment, or temporal instability in real-world scenarios. Moreover, some DM-based methods (*e.g.*, with DLoRAL [40] or DOVE [7]) tend to produce over-sharpened results that are less well aligned with



Figure 6. Temporal profiles on the real-world MVS4x dataset [46]. We select a row (yellow lines) and observe the changes across time.

Table 3. Complexity comparison among DM-based methods. All methods are evaluated on the same NVIDIA A800 GPU by generating a 97-frame 1024×1024 video with single-frame interpolation on MVS4x [46]. * DAM-VSR uses an extra DM of image super-resolution; only the main DM steps are reported.

Method	Diffusion Step	Inference Time (s)
LDMVFI [9] + DAM-VSR [25]	200 + 18*	1006 (348 + 658)
LDMVFI [9] + STAR [57]	200 + 15	854 (348 + 506)
LDMVFI [9] + DLoRAL [40]	200 + 1	469 (348 + 121)
LDMVFI [9] + DOVE [7]	200 + 1	414 (348 + 66)
EDEN [68] + DAM-VSR [25]	2 + 18*	668 (10 + 658)
EDEN [68] + STAR [57]	2 + 15	516 (10 + 506)
EDEN [68] + DLoRAL [40]	2 + 1	131 (10 + 121)
EDEN [68] + DOVE [7]	2 + 1	76 (10 + 66)
VEnhancer [16]	15	871
OSDEnhancer (Ours)	1	129

realistic details. In contrast, equipped with multi-scale deformable aggregation and inter-frame feature propagation in the decoder, OSDEnhancer achieves smoother temporal transitions while remaining more faithful to GT textures and structures.

Complexity Discussion. Tab. 3 compares diffusion steps and inference time for generating a 97-frame 1024×1024 video on MVS4x [46] using the same NVIDIA A800 GPU. Two-stage pipelines incur substantial latency due to multiple diffusion models with multi-step inference. Although replacing LDMVFI [9] with EDEN [68], which uses fewer diffusion steps, reduces the VFI cost, the overall runtime is still dominated by the subsequent VSR stage. In addition, VEnhancer [16] requires 15 diffusion steps for joint STVSR, leading to high inference time. Benefiting from a one-step diffusion framework, OSDEnhancer achieves lower latency with substantially improved efficiency while maintaining high restoration quality.

4.3. Ablation Study

To investigate the effectiveness of the proposed methodological design, we conduct ablation studies by maintaining the training protocols used in the main experiments and report PSNR for reconstruction fidelity, LPIPS [65] for perceptual quality, and FloLPIPS [8] for motion-aware temporal consistency on the UDM10 dataset [41].

TR-SE MoE. We first adopt the one-step adapted model from Stage 1 as the baseline (see Tab. 4), which is trained

Table 4. Ablation study on the TR-SE MoE. **Bold** indicates the best performance.

	PSNR \uparrow	LPIPS \downarrow	FloLPIPS \downarrow
Baseline	26.77	0.324	0.320
+ TR Expert	26.89	0.320	0.313
+ SE Expert	25.98	0.251	0.257
+ TR-SE MoE	26.44	0.248	0.253
Direct Fine-tuning	26.17	0.301	0.307

Table 5. Ablation study on the bidirectional deformable VAE decoder.

	PSNR \uparrow	LPIPS \downarrow	FloLPIPS \downarrow
Baseline	25.48	0.257	0.260
+ fwd. Compensation	26.11	0.253	0.253
+ bwd. Compensation	26.23	0.253	0.253
+ fwd. & bwd. Compensation	26.44	0.248	0.253
+ fwd. & bwd. Compensation (w/o DCN)	25.98	0.256	0.258
+ fwd. & bwd. Compensation (w/o lower offset)	26.31	0.254	0.256

only under spatial degradations and therefore generalizes poorly to scenarios involving temporal interpolation. Adding the TR expert enables explicit modeling of temporal degradations and substantially improves STVSR performance. However, both the baseline and the TR-only variant mainly rely on pixel-wise supervision, leading to inferior perceptual quality. When combining the baseline with only the SE expert, the perceptual metrics improve, but fidelity drops. In contrast, the full model with TR-SE MoE achieves the best LPIPS and FloLPIPS, demonstrating the complementary effects of the TR and SE experts. The qualitative results of different experts can be found in Fig. 1 (upper right). We also fine-tune the original DiT directly for one-step STVSR, which fails to converge to satisfactory performance, further highlighting the necessity of our design.

Bidirectional Deformable VAE Decoder. Tab. 5 reports the performance of different VAE decoder variants for STVSR. We first adopt the original VAE decoder [62] as the baseline. Introducing forward feature propagation leads to a clear performance improvement. Further incorporating backward propagation allows for the exploitation of future-frame information, resulting in more pronounced gains. When both forward and backward compensation are enabled, bidirectional information aggregation achieves the best overall performance. In addition, replacing deformable convolution and applying only cross-attention for inter-frame interaction degrades performance, as features from neighboring frames cannot be properly aligned with the current frame. Moreover, removing multi-scale offset aggregation also leads to performance drops, indicating its importance for effective spatiotemporal compensation.

Loss Configuration. Our OSDEnhancer involves different loss configurations in Stage 2 and Stage 3 to train the TR-SE MoE. The supervision for Stage 2 includes an MSE loss \mathcal{L}_{mse} and a residual-aware loss \mathcal{L}_{res} , with the results shown in Tab. 6. We can see that using only the pixel-wise re-

Table 6. Ablation study on loss configurations in Stage 2.

\mathcal{L}_{mse}	\mathcal{L}_{res}	PSNR \uparrow	LPIPS \downarrow	FloLPIPS \downarrow
✓		26.91	0.324	0.317
✓	✓	26.89	0.320	0.313

Table 7. Ablation study on loss configurations in Stage 3. All: all frequency components are involved in optical-flow warp loss; HF-only: only high-frequency components are involved.

\mathcal{L}_1	$\mathcal{L}_{\text{dists}}$	\mathcal{L}_{nqa}	$\mathcal{L}_{\text{warp}}$	PSNR \uparrow	LPIPS \downarrow	FloLPIPS \downarrow	MUSIQ \uparrow	DOVER \uparrow
✓				27.23	0.310	0.294	47.55	0.572
✓	✓			26.40	0.249	0.256	58.86	0.727
✓	✓	✓		26.45	0.255	0.260	64.98	0.780
✓	✓	✓	All	26.40	0.252	0.254	64.84	0.784
✓	✓	✓	HF-only	26.44	0.248	0.253	65.95	0.796

construction loss \mathcal{L}_{mse} achieves the highest PSNR, while adding the residual supervision \mathcal{L}_{res} slightly reduces PSNR but improves LPIPS and FloLPIPS, indicating better perceptual quality and temporal consistency. This suggests that residual modeling helps refine inter-frame details beyond strict pixel-wise fitting.

In Stage 3, in addition to the metrics reported in Tab. 6, we further report MUSIQ and DOVER in Tab. 7. Using only \mathcal{L}_1 achieves the best PSNR but results in inferior perceptual and temporal metrics, reflecting over-smoothed outputs. Adding the structural loss $\mathcal{L}_{\text{dists}}$ substantially improves LPIPS, MUSIQ, and DOVER. The further introduction of a no-reference quality assessment loss \mathcal{L}_{nqa} brings additional gains in perceptual and video quality. We also evaluate the optical-flow warping loss $\mathcal{L}_{\text{warp}}$ for temporal alignment. As we can see, applying it to all frequency components offers limited benefits, whereas restricting it to high-frequency components achieves the best overall performance across most metrics. This indicates that enforcing motion consistency primarily on high-frequency details better preserves fine structures and avoids over-constraining low-frequency regions, leading to superior performance.

5. Conclusion

In this paper, we present OSDEnhancer, an efficient one-step diffusion framework for real-world space-time video super-resolution (STVSR). By decomposing STVSR into temporal refinement and spatial enhancement through a mixture-of-experts design, our method enables specialized and collaborative modeling of temporal coherence and spatial details. A bidirectional deformable VAE decoder is further introduced to enhance cross-frame aggregation and compensation. Extensive experiments demonstrate superior fidelity and temporal consistency under complex real-world degradations, highlighting the potential of our method for practical applications.

References

- [1] Karlis Martins Briedis, Abdelaziz Djelouah, Raphaël Ortiz, Markus Gross, and Christopher Schroers. Controllable tracking-based video frame interpolation. In *Proceedings of the Special Interest Group on Computer Graphics and Interactive Techniques Conference Conference Papers*, pages 1–11, 2025. [2](#)
- [2] Jianrui Cai, Hui Zeng, Hongwei Yong, Zisheng Cao, and Lei Zhang. Toward real-world single image super-resolution: A new benchmark and a new model. In *Proceedings of the IEEE/CVF International Conference on Computer Vision*, pages 3086–3095, 2019. [6](#)
- [3] Kelvin CK Chan, Shangchen Zhou, Xiangyu Xu, and Chen Change Loy. Investigating tradeoffs in real-world video super-resolution. In *Proceedings of the IEEE/CVF Conference on Computer Vision and Pattern Recognition*, pages 5962–5971, 2022. [1, 2, 6, 7, 8, 15, 17](#)
- [4] Yi-Hsin Chen, Si-Cun Chen, Yen-Yu Lin, and Wen-Hsiao Peng. Motif: Learning motion trajectories with local implicit neural functions for continuous space-time video super-resolution. In *Proceedings of the IEEE/CVF International Conference on Computer Vision*, pages 23131–23141, 2023. [2, 3, 6, 7, 14](#)
- [5] Zeyuan Chen, Yinbo Chen, Jingwen Liu, Xingqian Xu, Vedit Goel, Zhangyang Wang, Humphrey Shi, and Xiaolong Wang. Videoinr: Learning video implicit neural representation for continuous space-time super-resolution. In *Proceedings of the IEEE/CVF Conference on Computer Vision and Pattern Recognition*, pages 2047–2057, 2022. [2, 3, 6, 7, 14](#)
- [6] Zhikai Chen, Fuchen Long, Zhaofan Qiu, Ting Yao, Wengang Zhou, Jiebo Luo, and Tao Mei. Learning spatial adaptation and temporal coherence in diffusion models for video super-resolution. In *Proceedings of the IEEE/CVF Conference on Computer Vision and Pattern Recognition*, pages 9232–9241, 2024. [3](#)
- [7] Zheng Chen, Zichen Zou, Kewei Zhang, Xiongfei Su, Xin Yuan, Yong Guo, and Yulun Zhang. Dove: Efficient one-step diffusion model for real-world video super-resolution. *arXiv preprint arXiv:2505.16239*, 2025. [2, 3, 6, 7, 8, 9, 14](#)
- [8] Duolikun Danier, Fan Zhang, and David Bull. Flolips: A bespoke video quality metric for frame interpolation. In *2022 Picture Coding Symposium*, pages 283–287. IEEE, 2022. [6, 9](#)
- [9] Duolikun Danier, Fan Zhang, and David Bull. Ldmvfi: Video frame interpolation with latent diffusion models. In *Proceedings of the AAAI Conference on Artificial Intelligence*, pages 1472–1480, 2024. [3, 6, 7, 9](#)
- [10] Keyan Ding, Kede Ma, Shiqi Wang, and Eero P Simoncelli. Image quality assessment: Unifying structure and texture similarity. *IEEE Transactions on Pattern Analysis and Machine Intelligence*, 44(5):2567–2581, 2020. [5](#)
- [11] Shian Du, Menghan Xia, Chang Liu, Xintao Wang, Jing Wang, Pengfei Wan, Di Zhang, and Xiangyang Ji. Patchvsr: Breaking video diffusion resolution limits with patch-wise video super-resolution. In *Proceedings of the IEEE/CVF Conference on Computer Vision and Pattern Recognition*, pages 17799–17809, 2025. [2](#)

[12] Patrick Esser, Sumith Kulal, Andreas Blattmann, Rahim Entezari, Jonas Müller, Harry Saini, Yam Levi, Dominik Lorenz, Axel Sauer, Frederic Boesel, et al. Scaling rectified flow transformers for high-resolution image synthesis. In *Proceedings of the 41st International Conference on Machine Learning*, 2024. 2

[13] Zhicheng Geng, Luming Liang, Tianyu Ding, and Ilya Zharkov. Rstt: Real-time spatial temporal transformer for space-time video super-resolution. In *Proceedings of the IEEE/CVF Conference on Computer Vision and Pattern Recognition*, pages 17441–17451, 2022. 3

[14] Janghyeok Han, Gyujin Sim, Geonung Kim, Hyun-Seung Lee, Kyuha Choi, Youngseok Han, and Sunghyun Cho. Dc-vsr: Spatially and temporally consistent video super-resolution with video diffusion prior. In *Proceedings of the Special Interest Group on Computer Graphics and Interactive Techniques Conference Conference Papers*, pages 1–11, 2025. 2, 3

[15] Muhammad Haris, Greg Shakhnarovich, and Norimichi Ukita. Space-time-aware multi-resolution video enhancement. In *Proceedings of the IEEE/CVF Conference on Computer Vision and Pattern Recognition*, pages 2859–2868, 2020. 3

[16] Jingwen He, Tianfan Xue, Dongyang Liu, Xinqi Lin, Peng Gao, Dahua Lin, Yu Qiao, Wanli Ouyang, and Ziwei Liu. Venhancer: Generative space-time enhancement for video generation. *arXiv preprint arXiv:2407.07667*, 2024. 1, 3, 6, 7, 9, 14

[17] Wenyi Hong, Ming Ding, Wendi Zheng, Xinghan Liu, and Jie Tang. Cogvideo: Large-scale pretraining for text-to-video generation via transformers. *arXiv preprint arXiv:2205.15868*, 2022. 2

[18] Edward J Hu, Yelong Shen, Phillip Wallis, Zeyuan Allen-Zhu, Yuanzhi Li, Shean Wang, Lu Wang, and Weizhu Chen. Lora: Low-rank adaptation of large language models. *arXiv preprint arXiv:2106.09685*, 2021. 5, 14

[19] Mengshun Hu, Kui Jiang, Zhixiang Nie, Jiahuan Zhou, and Zheng Wang. Store and fetch immediately: Everything is all you need for space-time video super-resolution. In *Proceedings of the AAAI Conference on Artificial Intelligence*, pages 863–871, 2023. 3

[20] Zhenwei Huang, Ailin Huang, Xiaotao Hu, Chen Hu, Jun Xu, and Shuchang Zhou. Scale-adaptive feature aggregation for efficient space-time video super-resolution. In *Proceedings of the IEEE/CVF winter conference on applications of computer vision*, pages 4228–4239, 2024. 3

[21] Junhwa Hur, Charles Herrmann, Saurabh Saxena, Janne Kontkanen, Wei-Sheng Lai, Yichang Shih, Michael Rubinstein, David J Fleet, and Deqing Sun. High-resolution frame interpolation with patch-based cascaded diffusion. In *Proceedings of the AAAI Conference on Artificial Intelligence*, pages 3868–3876, 2025. 2

[22] Siddhant Jain, Daniel Watson, Eric Tabellion, Ben Poole, Janne Kontkanen, et al. Video interpolation with diffusion models. In *Proceedings of the IEEE/CVF Conference on Computer Vision and Pattern Recognition*, pages 7341–7351, 2024. 2, 3

[23] Junjie Ke, Qifei Wang, Yilin Wang, Peyman Milanfar, and Feng Yang. Musiq: Multi-scale image quality transformer. In *Proceedings of the IEEE/CVF International Conference on Computer Vision*, pages 5148–5157, 2021. 5, 6

[24] Eunjin Kim, Hyeonjin Kim, Kyong Hwan Jin, and Jaejun Yoo. Bf-stvsr: B-splines and fourier—best friends for high fidelity spatial-temporal video super-resolution. In *Proceedings of the IEEE/CVF Conference on Computer Vision and Pattern Recognition*, pages 28009–28018, 2025. 2, 3, 6, 7, 14

[25] Zhe Kong, Le Li, Yong Zhang, Feng Gao, Shaoshu Yang, Tao Wang, Kaihao Zhang, Zhuoliang Kang, Xiaoming Wei, Guanying Chen, et al. Dam-vsr: Disentanglement of appearance and motion for video super-resolution. In *Proceedings of the Special Interest Group on Computer Graphics and Interactive Techniques Conference Conference Papers*, pages 1–11, 2025. 2, 3, 6, 7, 9

[26] Wei-Sheng Lai, Jia-Bin Huang, Oliver Wang, Eli Shechtman, Ersin Yumer, and Ming-Hsuan Yang. Learning blind video temporal consistency. In *Proceedings of the Proceedings of the European Conference on Computer Vision*, pages 170–185, 2018. 5, 14

[27] Jaihyun Lew, Jooyoung Choi, Chaehun Shin, Dahuin Jung, and Sungroh Yoon. Disentangled motion modeling for video frame interpolation. In *Proceedings of the AAAI Conference on Artificial Intelligence*, pages 4607–4615, 2025. 3

[28] Feng Li, Yixuan Wu, Anqi Li, Huihui Bai, Runmin Cong, and Yao Zhao. Enhanced video super-resolution network towards compressed data. *ACM Transactions on Multimedia Computing, Communications and Applications*, 20(7):1–21, 2024. 2

[29] Xiaohui Li, Yihao Liu, Shuo Cao, Ziyan Chen, Shaobin Zhuang, Xiangyu Chen, Yinan He, Yi Wang, and Yu Qiao. Diffvsr: Revealing an effective recipe for taming robust video super-resolution against complex degradations. In *Proceedings of the IEEE/CVF International Conference on Computer Vision*, pages 15319–15328, 2025. 2, 3

[30] Yong Liu, Jinshan Pan, Yinchuan Li, Qingji Dong, Chao Zhu, Yu Guo, and Fei Wang. Ultravsr: Achieving ultra-realistic video super-resolution with efficient one-step diffusion space. In *Proceedings of the 33rd ACM International Conference on Multimedia*, pages 7785–7794, 2025. 2, 3

[31] Ilya Loshchilov, Frank Hutter, et al. Fixing weight decay regularization in adam. *arXiv preprint arXiv:1711.05101*, 5(5):5, 2017. 14

[32] Seungjun Nah, Tae Hyun Kim, and Kyoung Mu Lee. Deep multi-scale convolutional neural network for dynamic scene deblurring. In *Proceedings of the IEEE/CVF Conference on Computer Vision and Pattern Recognition*, pages 3883–3891, 2017. 6, 7, 8, 16

[33] Jiaxin Peng, Siwang Zhou, Chengqing Li, Yucheng Li, and Dunyun Chen. Mitigating delivery artifacts in real-world video super-resolution. In *Proceedings of the 33rd ACM International Conference on Multimedia*, pages 3114–3123, 2025. 2

[34] Zhongwei Qiu, Huan Yang, Jianlong Fu, Daochang Liu, Chang Xu, and Dongmei Fu. Learning degradation-robust

spatiotemporal frequency-transformer for video super-resolution. *IEEE Transactions on Pattern Analysis and Machine Intelligence*, 45(12):14888–14904, 2023. 2

[35] Robin Rombach, Andreas Blattmann, Dominik Lorenz, Patrick Esser, and Björn Ommer. High-resolution image synthesis with latent diffusion models. In *Proceedings of the IEEE/CVF Conference on Computer Vision and Pattern Recognition*, pages 10684–10695, 2022. 2

[36] Wonyong Seo, Jihyong Oh, and Munchurl Kim. Bim-vfi: Bidirectional motion field-guided frame interpolation for video with non-uniform motions. In *Proceedings of the IEEE/CVF Conference on Computer Vision and Pattern Recognition*, pages 7244–7253, 2025. 2

[37] Liao Shen, Tianqi Liu, Huiqiang Sun, Xinyi Ye, Baopu Li, Jianming Zhang, and Zhiguo Cao. Dreammover: Leveraging the prior of diffusion models for image interpolation with large motion. In *Proceedings of the European Conference on Computer Vision*, pages 336–353. Springer, 2024. 2, 3

[38] Shijun Shi, Jing Xu, Lijing Lu, Zhihang Li, and Kai Hu. Self-supervised controlnet with spatio-temporal mamba for real-world video super-resolution. In *Proceedings of the IEEE/CVF Conference on Computer Vision and Pattern Recognition*, pages 7385–7395, 2025. 2

[39] Shuochen Su, Mauricio Delbracio, Jue Wang, Guillermo Sapiro, Wolfgang Heidrich, and Oliver Wang. Deep video deblurring for hand-held cameras. In *Proceedings of the IEEE/CVF Conference on Computer Vision and Pattern Recognition*, pages 1279–1288, 2017. 6

[40] Yujing Sun, Lingchen Sun, Shuaizheng Liu, Rongyuan Wu, Zhengqiang Zhang, and Lei Zhang. One-step diffusion for detail-rich and temporally consistent video super-resolution. In *The Thirty-ninth Annual Conference on Neural Information Processing Systems*, 2025. 2, 3, 6, 7, 8, 9

[41] Xin Tao, Hongyun Gao, Renjie Liao, Jue Wang, and Jaya Jia. Detail-revealing deep video super-resolution. In *Proceedings of the IEEE/CVF International Conference on Computer Vision*, pages 4472–4480, 2017. 6, 7, 9, 15

[42] Yuan Tian, Guo Lu, Xiongkuo Min, Zhaohui Che, Guangtao Zhai, Guodong Guo, and Zhiyong Gao. Self-conditioned probabilistic learning of video rescaling. In *Proceedings of the IEEE/CVF International Conference on Computer Vision*, pages 4490–4499, 2021. 2

[43] Jianyi Wang, Kelvin CK Chan, and Chen Change Loy. Exploring clip for assessing the look and feel of images. In *Proceedings of the AAAI Conference on Artificial Intelligence*, pages 2555–2563, 2023. 6

[44] Jianyi Wang, Shanchuan Lin, Zhijie Lin, Yuxi Ren, Meng Wei, Zongsheng Yue, Shangchen Zhou, Hao Chen, Yang Zhao, Ceyuan Yang, et al. Seedvr2: One-step video restoration via diffusion adversarial post-training. *arXiv preprint arXiv:2506.05301*, 2025. 2, 3

[45] Jianyi Wang, Zhijie Lin, Meng Wei, Yang Zhao, Ceyuan Yang, Chen Change Loy, and Lu Jiang. Seedvr: Seeding infinity in diffusion transformer towards generic video restoration. In *Proceedings of the IEEE/CVF Conference on Computer Vision and Pattern Recognition*, pages 2161–2172, 2025. 2

[46] Ruohao Wang, Xiaohui Liu, Zhilu Zhang, Xiaohu Wu, Chun-Mei Feng, Lei Zhang, and Wangmeng Zuo. Benchmark dataset and effective inter-frame alignment for real-world video super-resolution. In *Proceedings of the IEEE/CVF Conference on Computer Vision and Pattern Recognition*, pages 1168–1177, 2023. 1, 2, 6, 7, 9, 15

[47] Xintao Wang, Kelvin CK Chan, Ke Yu, Chao Dong, and Chen Change Loy. Edvr: Video restoration with enhanced deformable convolutional networks. In *Proceedings of the IEEE/CVF Conference on Computer Vision and Pattern Recognition workshops*, pages 0–0, 2019. 5

[48] Yang Wang, Yi Yang, Zhenheng Yang, Liang Zhao, Peng Wang, and Wei Xu. Occlusion aware unsupervised learning of optical flow. In *Proceedings of the IEEE/CVF Conference on Computer Vision and Pattern Recognition*, pages 4884–4893, 2018. 14

[49] Zhou Wang, Alan C Bovik, Hamid R Sheikh, and Eero P Simoncelli. Image quality assessment: from error visibility to structural similarity. *IEEE Transactions on Image Processing*, 13(4):600–612, 2004. 6

[50] Shuoyan Wei, Feng Li, Shengeng Tang, Yao Zhao, and Huihui Bai. Evenhancer: Empowering effectiveness, efficiency and generalizability for continuous space-time video super-resolution with events. In *Proceedings of the IEEE/CVF Conference on Computer Vision and Pattern Recognition*, pages 17755–17766, 2025. 2

[51] Haoning Wu, Chaofeng Chen, Liang Liao, Jingwen Hou, Wenxiu Sun, Qiong Yan, Jinwei Gu, and Weisi Lin. Neighbourhood representative sampling for efficient end-to-end video quality assessment. *IEEE Transactions on Pattern Analysis and Machine Intelligence*, 45(12):15185–15202, 2023. 6

[52] Haoning Wu, Erli Zhang, Liang Liao, Chaofeng Chen, Jingwen Hou, Annan Wang, Wenxiu Sun, Qiong Yan, and Weisi Lin. Exploring video quality assessment on user generated contents from aesthetic and technical perspectives. In *Proceedings of the IEEE/CVF International Conference on Computer Vision*, pages 20144–20154, 2023. 6

[53] Rongyuan Wu, Lingchen Sun, Zhiyuan Ma, and Lei Zhang. One-step effective diffusion network for real-world image super-resolution. *Advances in Neural Information Processing Systems*, 37:92529–92553, 2024. 3

[54] Rongyuan Wu, Tao Yang, Lingchen Sun, Zhengqiang Zhang, Shuai Li, and Lei Zhang. Seesr: Towards semantics-aware real-world image super-resolution. In *Proceedings of the IEEE/CVF Conference on Computer Vision and Pattern Recognition*, pages 25456–25467, 2024. 3

[55] Xiaoyu Xiang, Yapeng Tian, Yulun Zhang, Yun Fu, Jan P Allebach, and Chenliang Xu. Zooming slow-mo: Fast and accurate one-stage space-time video super-resolution. In *Proceedings of the IEEE/CVF Conference on Computer Vision and Pattern Recognition*, pages 3370–3379, 2020. 2, 3

[56] Zeyu Xiao, Zhiwei Xiong, Xueyang Fu, Dong Liu, and Zheng-Jun Zha. Space-time video super-resolution using temporal profiles. In *Proceedings of the 28th ACM International Conference on Multimedia*, pages 664–672, 2020. 2

[57] Rui Xie, Yinhong Liu, Penghao Zhou, Chen Zhao, Jun Zhou, Kai Zhang, Zhenyu Zhang, Jian Yang, Zhenheng Yang, and Ying Tai. Star: Spatial-temporal augmentation with text-to-video models for real-world video super-resolution. In *Proceedings of the IEEE/CVF International Conference on Computer Vision*, pages 17108–17118, 2025. 3, 6, 7, 9

[58] Gang Xu, Jun Xu, Zhen Li, Liang Wang, Xing Sun, and Ming-Ming Cheng. Temporal modulation network for controllable space-time video super-resolution. In *Proceedings of the IEEE/CVF Conference on Computer Vision and Pattern Recognition*, pages 6388–6397, 2021. 2, 3

[59] Yiran Xu, Taesung Park, Richard Zhang, Yang Zhou, Eli Shechtman, Feng Liu, Jia-Bin Huang, and Difan Liu. Videogigagan: Towards detail-rich video super-resolution. In *Proceedings of the IEEE/CVF Conference on Computer Vision and Pattern Recognition*, pages 2139–2149, 2025. 2

[60] Serin Yang, Taesung Kwon, and Jong Chul Ye. Vibidsampler: Enhancing video interpolation using bidirectional diffusion sampler. *arXiv preprint arXiv:2410.05651*, 2024. 2, 3

[61] Xi Yang, Chenhang He, Jianqi Ma, and Lei Zhang. Motion-guided latent diffusion for temporally consistent real-world video super-resolution. In *Proceedings of the European Conference on Computer Vision*, pages 224–242. Springer, 2024. 2, 3

[62] Zhuoyi Yang, Jiayan Teng, Wendi Zheng, Ming Ding, Shiyu Huang, Jiazheng Xu, Yuanming Yang, Wenyi Hong, Xiaohan Zhang, Guanyu Feng, et al. Cogvideox: Text-to-video diffusion models with an expert transformer. *arXiv preprint arXiv:2408.06072*, 2024. 2, 3, 5, 6, 9

[63] Peng Yi, Zhongyuan Wang, Kui Jiang, Junjun Jiang, and Jiayi Ma. Progressive fusion video super-resolution network via exploiting non-local spatio-temporal correlations. In *Proceedings of the IEEE/CVF International Conference on Computer Vision*, pages 3106–3115, 2019. 6, 7, 15

[64] Lvmiin Zhang, Anyi Rao, and Maneesh Agrawala. Adding conditional control to text-to-image diffusion models. In *Proceedings of the IEEE/CVF International Conference on Computer Vision*, pages 3836–3847, 2023. 3

[65] Richard Zhang, Phillip Isola, Alexei A Efros, Eli Shechtman, and Oliver Wang. The unreasonable effectiveness of deep features as a perceptual metric. In *Proceedings of the IEEE/CVF Conference on Computer Vision and Pattern Recognition*, pages 586–595, 2018. 6, 9

[66] Yuehan Zhang and Angela Yao. Realvifomer: Investigating attention for real-world video super-resolution. In *Proceedings of the European Conference on Computer Vision*, pages 412–428. Springer, 2024. 2

[67] Yuantong Zhang, Hanyou Zheng, Daiqin Yang, Zhenzhong Chen, Haichuan Ma, and Wengpeng Ding. Space-time video super-resolution with neural operator. *IEEE Transactions on Image Processing*, 2025. 2

[68] Zihao Zhang, Haoran Chen, Haoyu Zhao, Guansong Lu, Yanwei Fu, Hang Xu, and Zuxuan Wu. Eden: Enhanced diffusion for high-quality large-motion video frame interpolation. In *Proceedings of the IEEE/CVF Conference on Computer Vision and Pattern Recognition*, pages 2105–2115, 2025. 3, 6, 7, 9

[69] Shangchen Zhou, Peiqing Yang, Jianyi Wang, Yihang Luo, and Chen Change Loy. Upscale-a-video: Temporal-consistent diffusion model for real-world video super-resolution. In *Proceedings of the IEEE/CVF Conference on Computer Vision and Pattern Recognition*, pages 2535–2545, 2024. 2, 3, 6, 7, 15

[70] Tianyi Zhu, Dongwei Ren, Qilong Wang, Xiaohe Wu, and Wangmeng Zuo. Generative inbetweening through frame-wise conditions-driven video generation. In *Proceedings of the IEEE/CVF Conference on Computer Vision and Pattern Recognition*, pages 27968–27978, 2025. 2, 3

[71] Xizhou Zhu, Han Hu, Stephen Lin, and Jifeng Dai. Deformable convnets v2: More deformable, better results. In *Proceedings of the IEEE/CVF Conference on Computer Vision and Pattern Recognition*, pages 9308–9316, 2019. 5

[72] Junhao Zhuang, Shi Guo, Xin Cai, Xiaohui Li, Yihao Liu, Chun Yuan, and Tianfan Xue. Flashvsr: Towards real-time diffusion-based streaming video super-resolution. *arXiv preprint arXiv:2510.12747*, 2025. 3

OSDEnhancer: Taming Real-World Space-Time Video Super-Resolution with One-Step Diffusion

Supplementary Material

This appendix contains supplementary materials related to the proposed OSDEnhancer. The structure of the supplementary materials is organized as follows:

- Implementation details of OSDEnhancer (Sec. A)
- Definitions of loss terms (Sec. B)
- Additional qualitative comparisons (Sec. C)

A. Implementation Details

We first pre-train the bidirectional deformable VAE decoder independently to obtain a stable latent-to-pixel reconstruction. The VAE decoder is trained for 5,000 iterations with a learning rate of 1×10^{-4} on video sequences of 33 frames at a resolution of 256×256 . To achieve a better trade-off between reconstruction fidelity and perceptual quality, we adopt the diffusion timestep setting recommended by previous work [7], *i.e.*, $t = 399$. In Stages 1–2, we train on video sequences of 33 frames at a resolution of 320×640 , performing 15,000 iterations with a learning rate of 2×10^{-5} in Stage 1 and 10,000 iterations with a learning rate of 1×10^{-4} and $\lambda_{\text{res}} = 1$ in Stage 2. In Stage 3, we use 9-frame video/image sequences at a resolution of 320×320 and train for 5,000 iterations with a learning rate of 5×10^{-5} . The loss weights λ_{dists} , λ_{warp} , and λ_{nqa} are set to 1, 0.05, and 0.05, respectively. All stages are optimized using the AdamW optimizer [31] with $\beta_1 = 0.9$ and $\beta_2 = 0.95$. For both TR and SE experts, we inject LoRA adapters [18] into the DiT, covering the query, key, value, and output projections of 3D attention and the projection layers of the feed-forward networks. For the SE expert, we further inject LoRA into the final output projection layer. All LoRA modules use rank $r = 128$ with a scaling factor $\alpha = 128$.

B. Definitions of Loss Terms

Here, we provide detailed formulations of the residual loss \mathcal{L}_{res} and the self-supervised optical-flow warping loss $\mathcal{L}_{\text{warp}}$ [26].

The residual loss \mathcal{L}_{res} in latent/pixel space:

$$\mathcal{L}_{\text{res}} = \frac{1}{L_{\text{lat}} - 1} \sum_{j=1}^{L_{\text{lat}}-1} \|(z_{j+1}^{\text{out}} - z_j^{\text{out}}) - (z_{j+1}^{\text{gt}} - z_j^{\text{gt}})\|, \quad (10)$$

$$\mathcal{L}_{\text{res}} = \frac{1}{L_{\text{pix}} - 1} \sum_{j=1}^{L_{\text{pix}}-1} \|(I_{j+1}^{\text{out}} - I_j^{\text{out}}) - (I_{j+1}^{\text{gt}} - I_j^{\text{gt}})\|, \quad (11)$$

where $z_j^{\text{out}} \in \mathbf{z}^{\text{out}}$, $z_j^{\text{gt}} \in \mathbf{z}^{\text{gt}}$, $I_j^{\text{out}} \in \mathbf{I}^{\text{out}}$, and $I_j^{\text{gt}} \in \mathbf{I}^{\text{gt}}$; L_{lat} and L_{pix} are the lengths of the latent and frame sequences, respectively.

The self-supervised optical-flow warping loss $\mathcal{L}_{\text{warp}}$ in pixel space:

$$\mathcal{L}_{\text{warp}} = \frac{1}{L_{\text{pix}} - 1} \sum_{j=1}^{L_{\text{pix}}-1} \frac{\|\hat{M}_j \odot (\hat{O}_{j \rightarrow j+1}(H_j^{\text{out}}) - H_{j+1}^{\text{out}})\|}{\|\hat{M}_j\| + \xi}, \quad (12)$$

where $\hat{O}_{j \rightarrow j+1}$ denotes the warping operator induced by the optical flow from I_j^{out} to I_{j+1}^{out} , while \hat{M}_j is the non-occlusion mask constructed via forward–backward consistency [48] to ignore occluded and out-of-bounds regions; H_j^{out} is the high-frequency component of I_j^{out} , and ξ is a small constant introduced to avoid division by zero.

C. More Qualitative Comparisons

More qualitative comparisons on synthesis datasets and real-world datasets are illustrated in Fig. 7 and Fig. 8, respectively. Furthermore, we conduct qualitative comparisons with state-of-the-art continuous STVSR methods [4, 5, 16, 24] on arbitrary spatiotemporal scales. As shown in Fig. 9, we evaluate a highly challenging out-of-distribution setting with $8 \times$ spatial upscaling and 11-frame interpolation. Benefiting from a stronger diffusion prior and unified spatiotemporal compensation, OSDEnhancer demonstrates better generalization, achieving more temporally consistent results with higher reconstruction fidelity and perceptual quality. In addition, we fix the input resolution and perform arbitrary-scale spatial upscaling (from $4 \times$ to $8 \times$) with single-frame interpolation. As illustrated in Fig. 10, our method achieves the best performance in terms of structural stability and richness of details.

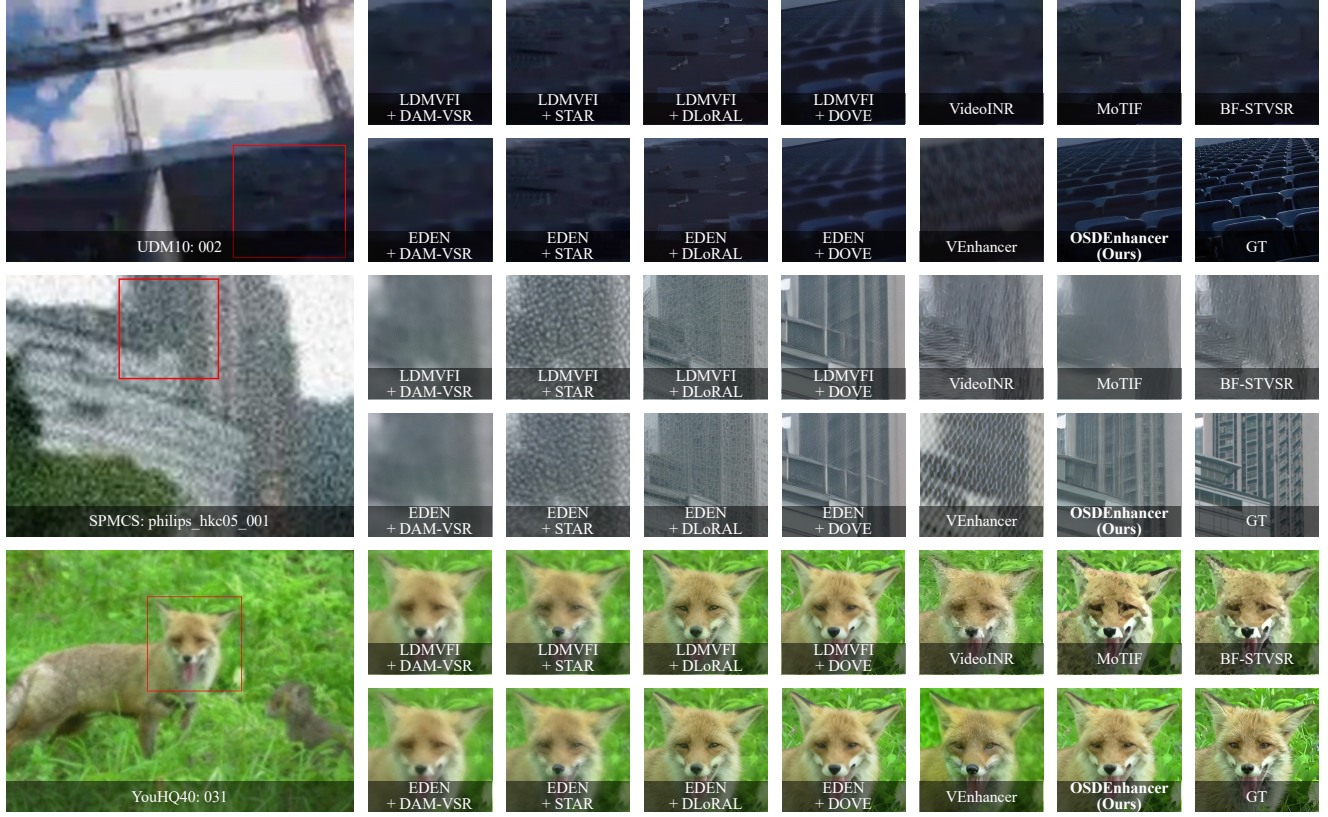


Figure 7. Qualitative comparison of interpolated frames on synthesis videos from UDM10 [41], SPMCS [63], and YouHQ40 [69]. Left: overlay of adjacent LR frames.

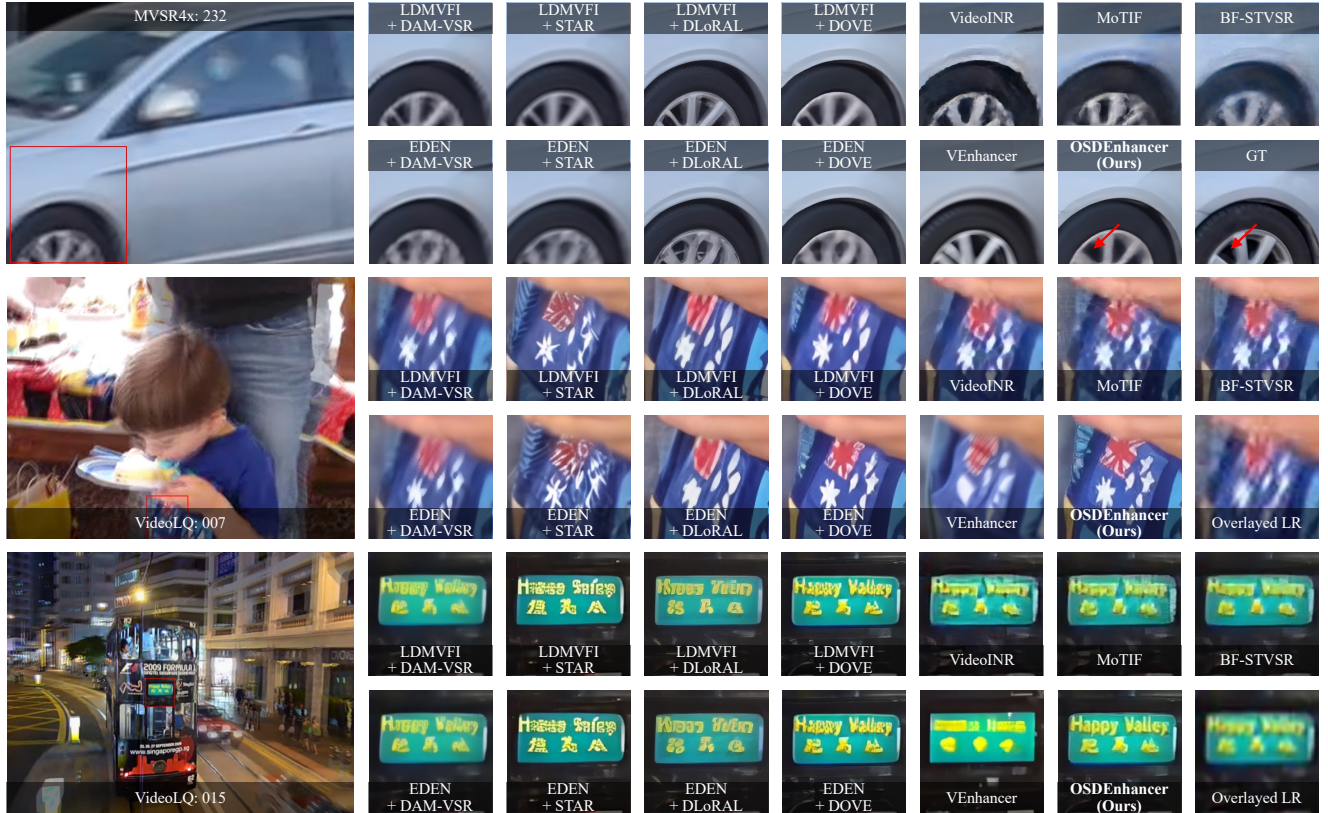


Figure 8. Qualitative comparison of interpolated frames on real-world videos from MVSR4x [46] and VideoLQ [3]. Left: overlay of adjacent LR frames.

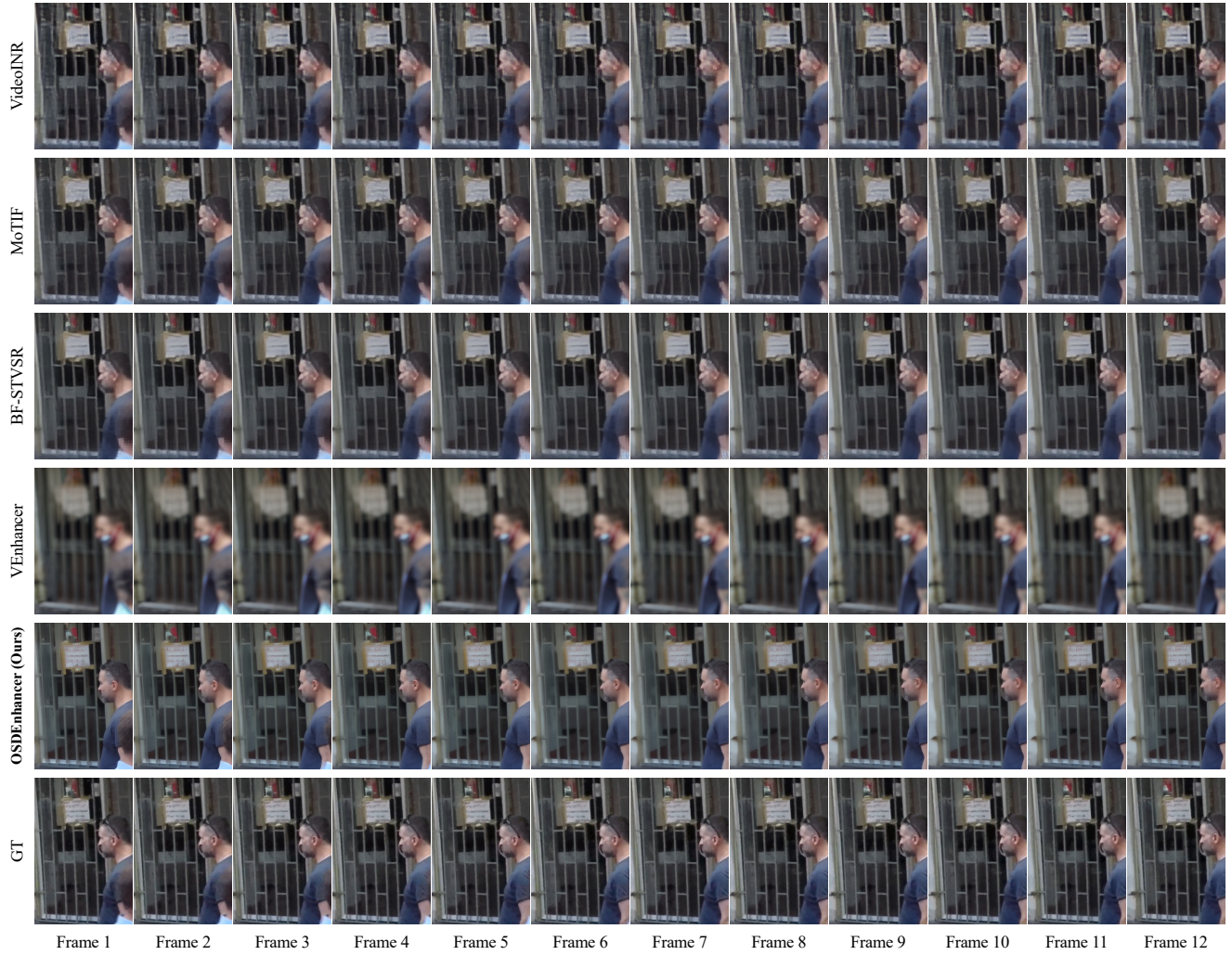


Figure 9. Qualitative comparison of STVSR on the GoPro dataset [32] with 8 \times spatial upscaling and 11-frame interpolation (frames 2–12 are interpolated).

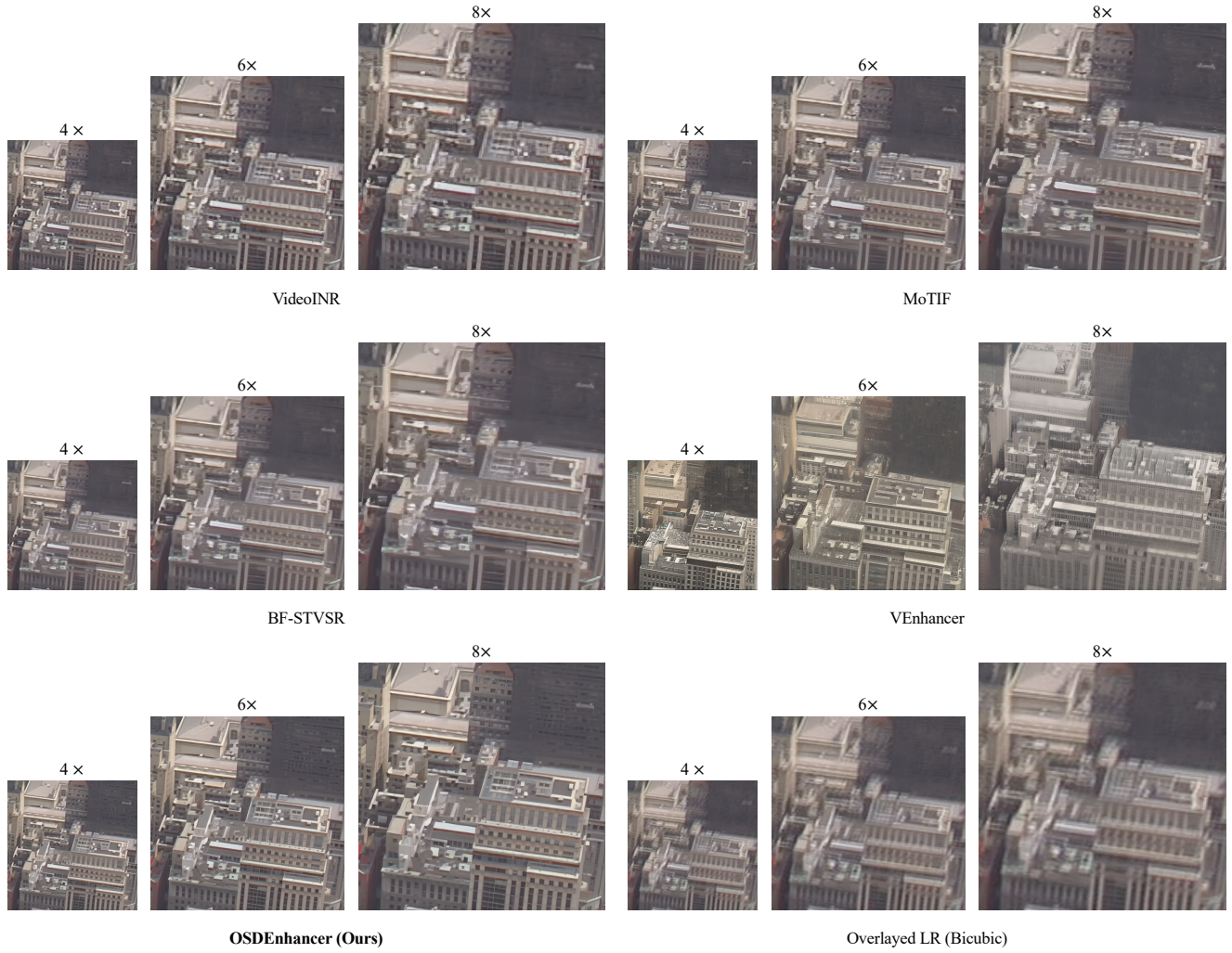


Figure 10. Qualitative comparison of interpolated frames with spatial upscaling of $4\times$, $6\times$, and $8\times$ on real-world videos from VideoLQ [3].